



Surface porous carbon nanofibers based on coaxial electrospinning with improved mechanical strength and cycle stability for freestanding anode in Li-ion batteries

Chao Zhang¹, Jun Yan¹, Rui Song¹, Lei Chen^{1,*} , and Yong Liu¹

¹ School of Textile Science and Engineering, Tiangong University, Tianjin 300387, China

Received: 28 May 2021

Accepted: 13 September 2021

Published online:
20 September 2021

© The Author(s), under exclusive licence to Springer Science+Business Media, LLC, part of Springer Nature 2021

ABSTRACT

Porous carbon nanofibers (PCNFs), are widely used as free-standing anode materials for lithium-ion batteries (LIBs), due to their high specific surface area and excellent ion diffusion kinetics, but they also present problems of reduced rate performance and cycling performance, due to poor strength caused by porosity. Herein, a novel surface porous carbon nanofiber (SPCNFs) is prepared by coaxial electrospinning, followed by carbonization. All the pores are distributed in the shell of the fibers, with a dense amorphous carbon structure in the core, which would not only provide abundant lithium-ion embedding sites, and accelerate the penetration of electrolyte ions, but also alleviate the reduction of mechanical properties (with a $\sim 30\%$ improvement to PCNFs). Consequently, our LIBs assembled with this SPCNFs anode represent remarkable cycling stability ($445.33 \text{ mAh g}^{-1}$ at 100 mA g^{-1} after 100 cycles and $388.92 \text{ mAh g}^{-1}$ at 1 A g^{-1} after 1000 cycles), and excellent rate capacity ($317.55 \text{ mAh g}^{-1}$ at 1 A g^{-1}).

Introduction

In 2019, the Royal Swedish Academy of Science awarded the Nobel Prize in Chemistry 2019 to three scientists, for their outstanding contributions in the development of lithium-ion batteries (LIBs). With the continuous decline of unsustainable resources, such as crude oil, coal, and minerals, the invention and

steady improvement of rechargeable LIBs give hope in enabling a fossil fuels-free society. However, due to the limited capacity (372 mAh g^{-1}), commercial LIBs graphite anode seems to meet a bottleneck in satisfying the requirements of the next-generation energy storage system [1, 2]. Carbon nanomaterials are considered the next generation of LIBs, due to their high specific surface area, good contact with the electrolyte, and fast electrochemical power [3, 4].

Handling Editor: Mark Bissett.

Address correspondence to E-mail: chenlei@tiangong.edu.cn

Electrospinning technology is widely used in the preparation of nanofibers, because of its low cost and good fiber uniformity [5, 6]. There are many precursor materials of carbon fiber, among which Polyacrylonitrile (PAN)-based carbon fiber has been widely used in the carbon fiber market, because of its relatively simple production process, and the same performance as other raw silk [7–10].

Chen et al. used a simple and scalable electrostatic spinning process and heat treatment to fabricate CNFs, and investigated their sodium storage mechanisms [11]. Therefore, the preparation of carbon nanofibers (CNFs) by electrospinning with the PAN as a spinning solution and high-temperature treatment by a program, is widely studied and applied to lithium-ion battery electrode materials. However, when CNFs are directly applied to lithium-ion battery anode, it is faced with the disadvantages of slow speed and low coulomb efficiency [12, 13]. To solve this problem, a large number of studies have focused on the metal doping and structural transformation of CNFs. Jiang et al. synthesized Co_9S_8 nanoparticles embedded in amorphous carbon by a simple electrostatic spinning method and high-temperature annealing process, showing excellent high lithium storage capacity [14]. Porous structures are even more widely studied, and various special shapes of CNFs have been prepared, such as hollow-CNFs [15, 16], porous-CNFs(PCNFs) [17, 18], etc.

The preparation of porous-CNFs has drawn attention in the application in LIBs anodes, which are believed to increase the high specific surface area and hydrophilicity, and provide more active sites for lithium ions, and then accelerate the migration of the electrolyte ions [19–22]. However, lots of works indicate that most of the effective pores in improving the electrochemical properties of CNFs, are located on the outer layer of the CNFs, because of the limited penetration of electrolytes due to the dense structure of not only graphite, but also amorphous carbon in CNFs. Rational design of meso-/micro-pores for enhancing ion transportation in highly-porous carbon nanofibers, used as an electrode for supercapacitors. Thus, the pores in the inner layer of CNFs would not supply active sites for lithium ions, but conversely, they will reduce the mechanical properties of CNFs, and consequently affect the rate properties and cycle performances negatively [14]. The preparation of PCNFs with a reasonable distribution of pores and ideal mechanical properties, has been an

attractive issue to improve the long-cycle stability of CNFs.

Coaxial electrospinning, also called two-fluid electrospinning, is widely developed as a promising strategy for the facile preparation of core-shell nanofibers, and their surface functionalization [23, 24]. The set-up is composed of two different coaxial capillary injectors with different solutions inside them, releasing the polymer fluids in the form of core-shell structure from the joint injector under an intense electrostatic field, starting at the tip. It shows great prospects in preparing nanofibers and their derivatives with distinct structures and performances for inner and outer layers. Liu et al. prepared a core-shell N-doped C@SnO₂ hybrid paper without binder and conductive additives by a coaxial electrostatic spinning method, and used it as an anode for LIBs, exhibiting excellent electrochemical properties [25]. In our previous work, coaxial electrospinning is used to fabricate a root-whisker structured CNFs-CNTs free-standing anode, which shows great affinity with electrolytes, and boosts the electrochemical kinetics, due to the precise catalyst deposition on the outer layer [26, 27].

Herein, we propose a surface porous carbon nanofiber (SPCNFs) structure, which is prepared by coaxial electrospinning and programmed heat treatment. The fibers have two layers, the inner layer is dense carbon, while the outer layer of a porous carbon structure. Because of its unique solid inner layer and improved mechanical properties, the surface porous electrode is more stable in the process of high current and long-cycle constant current charge and discharge process. This work not only provides a new method for the construction of carbon nanomaterials with different internal structures, but also supplies a novel strategy for improving the specific capacity of LIBs based on porous CNFs anodes, without damaging their mechanical properties and cycle performances.

Experiment

Materials

Polyacrylonitrile (PAN, $M_w = 150,000$) was bought from Chongqing Zhongna technology co. LTD. China. N, N-dimethylformamide (DMF) was bought from Shanghai Aladdin biochemical technology co.,

LTD.China. Polymethyl methacrylate (PMMA) was bought from Shanghai Macklin Biochemical Co., Ltd.

Preparation of surface porous carbon nanofiber membranes

Synthesis of PAN@PMMA/PAN nanofiber membranes using coaxial electrospinning technology. A clear solution was obtained, by dissolving 1.5 g PAN powder in 16 g DMF and stirring. Then, three different outer layer solutions were prepared by adding 3.5 g (PAN: PMMA = 3:7), 1.5 g (PAN: PMMA = 5:5), and 0.64 g (PAN: PMMA = 7:3) of PMMA by mass, respectively. 3 g of PAN powder was dissolved in 22 g DMF to obtain the inner layer solution. Homogeneous solutions were both obtained through stirred at 55 °C for 12 h under magnetic force. The electrospun films were collected by aluminum foil at the voltage of 12–18 kV and dried at 60 °C for 24 h. The as-prepared PAN@PMMA/PAN fibers were first stabilized at 270 °C for 1 h in air. Then, the fabricated samples were placed in a tube furnace, and carbonized for 2 h at 800 °C in nitrogen to obtain surface porous carbon nanofiber membranes (SPCNFs). Based on the content of PMMA in the spinning precursor, the three obtained films are denoted as SPCNFs-3:7, SPCNFs-5:5, SPCNFs-7:3. For comparison, porous carbon nanofibers(PCNFs) were prepared by uniaxial spinning technique, according to the ratio of the outer layer solution, and were noted as PCNFs-3:7, PCNFs-5:5, PCNFs-7:3, and the carbon nanofibers (CNFs) are obtained by direct carbonization of PAN films with a mass fraction of 12% under the same conditions.

Preparation and testing of the electrodes

The SPCNFs-5:5 film was directly used as an anode without assistant adhesives and conductive agents. The Celgard 2400 has been adopted as the separator. CR2025 coin cells were assembled in a glove box filled with argon ($H_2O < 0.1$ ppm, $O_2 < 0.1$ ppm), and the electrolyte were 1 M LiPF₆ in ethylene carbonate (EC), diethyl carbonate (DEC), and ethyl methyl carbonate (EMC) with 5% fluoroethylene carbonate (EC: DEC: EMC = 1:1:1). The cyclic voltammetry (CV) tests were conducted by CHI760E electrochemical workstation, at a scan rate of 0.1 mV s⁻¹. Galvanostatic charge/discharge cycles, were performed by a Wu-Han LAND CT3001A battery test system, in

a voltage range of 0.01–3.0 V. Electrochemical impedance spectroscopy (EIS) measured by the CHI760E in the frequency range from 100 kHz to 0.01 Hz, and the amplitude is 5 mV. All the capacities are calculated according to the total mass of the anode.

Material characterization

The surface morphology and internal structure of the obtained films, were characterized using field emission scanning electron microscopy (SEM), high-resolution transmission electron microscopy (HRTEM), and X-ray diffractometry (XRD). The mechanical properties of the membranes were evaluated, using a universal strong machine. The specific surface area was determined by the Brunauer–Emmett–Teller (BET) method.

Results and discussion

Structure and morphology of surface porous carbon nanofibers

Figure 1 depicts the detailed mechanism of the formation of such nanostructures. Firstly, both spinning solutions enter the coaxial needle at the same time, the inner layer is a PAN solution, and the outer layer is a homogeneous mixture of PAN and PMMA. PAN was the carbon source, and PMMA was the porogenic agent. Secondly, the film is pre-oxidized in a blast oven to make it resistant to high temperatures. Thirdly, carbon nanofibers are obtained by cleavage of PMMA in the carbonization process [28, 29].

There is a clear two-phase incompatibility between PAN and PMMA, so that the outer spinning liquid obtained after stirring has a clear two-phase interface, and is loosely connected [30]. Under the drawing of an applied electric field, the PMMA is drawn together and cleaved at high temperatures in a nitrogen atmosphere to form continuous pores. Firstly, the interlaced fiber network provides faster power and ion transport channels. Secondly, the inner layer solution is designed as a 12% mass fraction PAN solution, which is carbonized to provide strong support for the porous CNFs on the surface, ensuring the structural integrity of the anode during cycling, and improving cycling performance and reversible electrochemical reactions. Furthermore, the outer layer porous structure is believed to provide a high specific

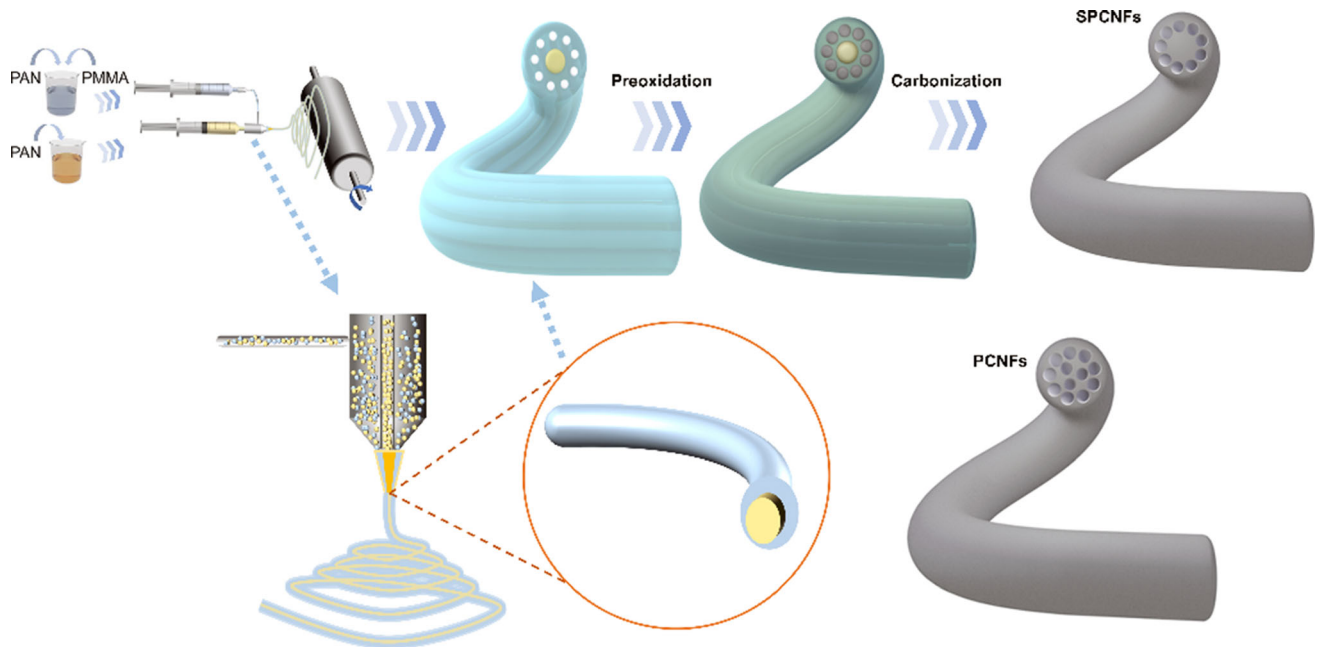


Figure 1 Schematic illustration of the fabrication procedure for SPCNFs.

surface area, increasing the wettability of the electrolyte, and providing more active sites for the embedding of lithium ions [13, 31].

Figure 2a–e shows the SEM images of CNFs, PCNFs-5:5, SPCNFs-5:5, and their corresponded cross-sectional views. In Fig. 2a, the normal CNFs are randomly distributed to form an interwoven network. All nanofibers show a smooth surface and a uniform diameter distribution of about 300 nm. However, the fiber diameters show a slight increase for both PCNFs and SPCNFs, after introducing holes. Furthermore, the surfaces are not smooth anymore, which should be attributed to the collapse of the fiber structure, resulted in forming of pores. Fortunately, due to the retaining of the dense and solid carbon structure of the inner layer for SPCNFs, the damage of fibers seems to be relieved (Fig. 2c). Figure 2d, e reveals the cross-sectional structure of PCNFs-5:5 and SPCNFs-5:5. Comparing with PCNFs, all of the holes are formed at the outer layer of SPCNFs, due to the arranged distribution of porogenic agent PMMA at the outer of the spinning solution based on the coaxial technique.

The HRTEM images, further depict more structural details of the SPCNFs-5:5 composite. Figure 3f shows the HRTEM and selected area electron diffraction (SAED) images of SPCNFs. Instead of a clear diffraction ring in the center of the transmission spot,

a diffuse halo spot appears, indicating that the surface porous structure produced by the template method, i.e., cleavage of PMMA, does not affect the crystallinity of the CNFs, which are still composed of amorphous carbon [32, 33].

Figure 2g–i shows the SPCNFs prepared at different ratios of PMMA content in the outer layer. As can be observed in Fig. 2g, when PAN: PMMA = 3:7, the fiber surface shows deep grooves, which are produced by the thermal cleavage of PMMA. This is due to the significant incompatibility between the two phases of the spinning solution, when the PMMA ratio is large, with more PMMA particles forming aggregates during the spinning process, and cleaving to produce larger diameter pores [34]. As the PMMA ratio decreases, the holes on the fiber surface tend to close, and become gradually smoother. As shown in Fig. 2h, when PAN: PMMA = 5:5, a core–shell structure can be observed, showing ring-like pores. This surface porous structure produces both distinct pores and maximum retention of the strength of the fiber [35]. As can be seen in Fig. 2i, when PAN: PMMA = 7:3, the fiber surface is smooth as that of CNFs, which may be induced by a little porous structure inside. Thus, we choose the sample with the ratio of PAN: PMMA = 5:5, for further investigation of their structures and mechanical and electrochemical performances. Such a structure provides more

Figure 2 SEM images of **a** CNFs, **b** PCNFs-5:5, **c** SPCNFs-5:5, **d** Cross-sectional view of PCNFs-5:5, **e** Cross-sectional view of SPCNFs-5:5. **f** HRTEM images of SPCNFs-5:5. SEM images of **g** SPCNFs-3:7, **h** SPCNFs-5:5, **i** SPCNFs-7:3.

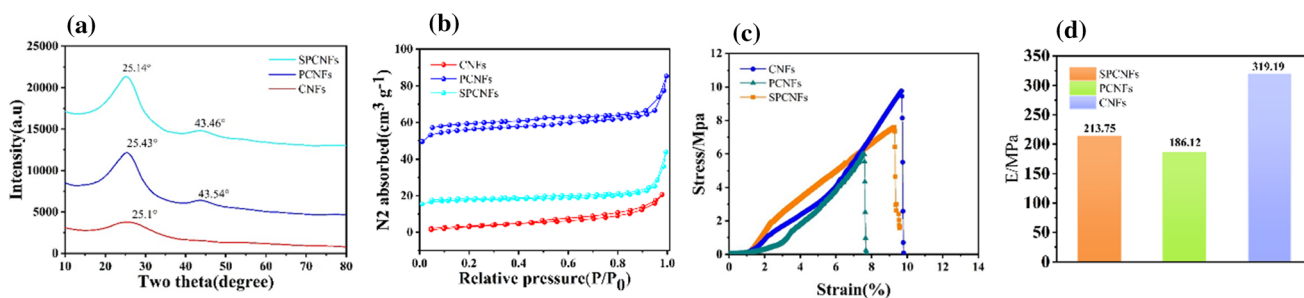
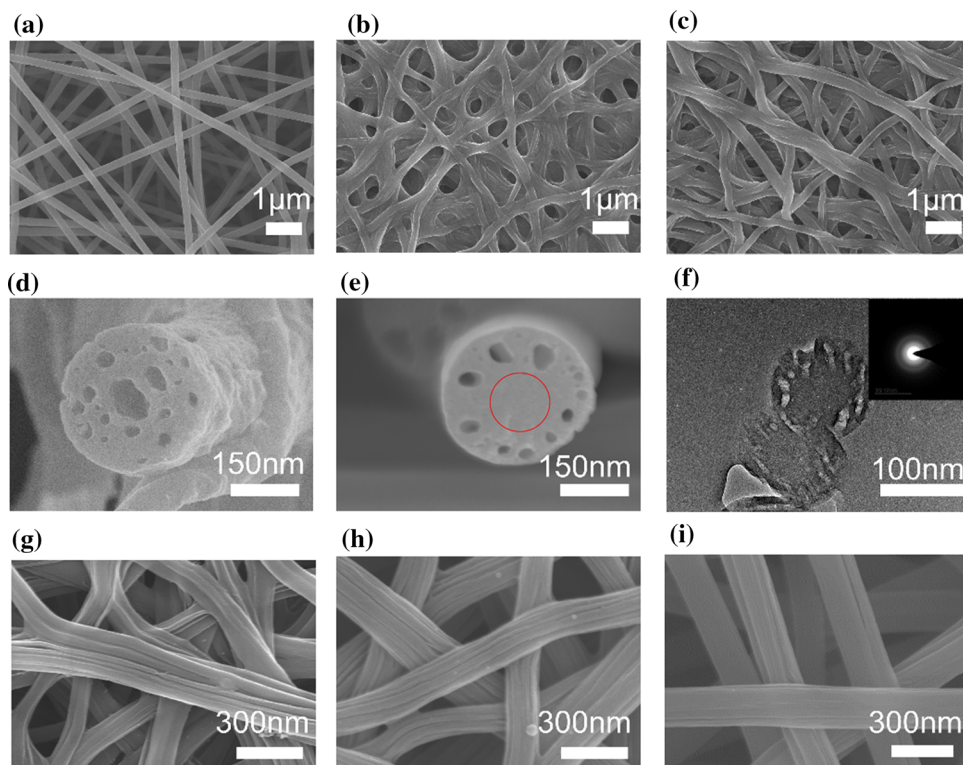


Figure 3 **a** XRD patterns of CNFs, PCNFs-5:5, and SPCNFs-5:5. **b** N_2 adsorption–desorption isotherm of CNFs, PCNFs-5:5 and SPCNFs-5:5. **c** Stress–strain curves of CNFs, PCNFs-5:5, and SPCNFs-5:5, **d** elastic modulus of SPCNFs-5:5, PCNFs-5:5 and CNFs.

active sites for the embedding of lithium ions, but also maximizes the stability of the structure, and improves the cycling stability of the electrode material during charging and discharging.

Figure 3a shows the XRD patterns of CNFs, PCNFs-5:5, and SPCNFs-5:5. The peaks of CNFs, PCNFs-5:5, and SPCNFs-5:5 at 2θ about 25° correspond to (002) graphitized layer, and PCNFs-5:5 and SPCNFs-5:5 show a peak at 2θ about 43.5° that is not obvious in CNFs, corresponding to the carbon surface of (100) turbocharged layer, indicating the appearance of a partially graphitized structure, which may be due to the rearrangement of the microstructure of PMMA during thermal cracking,

and the change in the layer order of the turbocharged layer [22, 36, 37].

The N_2 adsorption–desorption isotherms for CNFs, PCNFs-5:5, and SPCNFs-5:5 are shown in Fig. 3b. The specific surface areas of CNFs, PCNFs-5:5, and SPCNFs-5:5, were 13.46 , 81.34 , and $56.70 \text{ m}^2 \text{ g}^{-1}$, respectively. The significant increase in specific surface area was attributed to the formation of a large number of pores by thermal cracking of PMMA [38]. CNFs have the greatest tensile rupture strength, but SPCNFs-5:5 have better tensile rupture strength than PCNFs-5:5, probably due to the generation of porous structures that reduce the ability of the fibers to resist deformation. Figure 3d shows the elastic modulus of

the three fiber films, SPCNFs-5:5, PCNFs-5:5, and CNFsde modulus of 213.75, 186.12, and 319.19 MPa, respectively, demonstrating that the tensile strength of SPCNFs-5:5 was improved, compared to PCNFs. SPCNFs-5:5 combines the advantages of both, with the inner structure providing strength, and the outer pore structure providing the Li^+ embedding sites [34, 39].

Electrochemical performance

Figure 4a shows the EIS analysis for the different electrodes. EIS can reflect the charge transfer impedance and ion diffusion kinetics during lithium-ion storage. As can be seen from the diagram, the Nyquist plots for the different scales of electrode materials all consist of a semicircle in the high-frequency region and a sloping line in the low-frequency region. The semicircle in the high-frequency region corresponds to the migration resistance, resulting from the passage of Li^+ through the SEI layer process and the charge transfer resistance at the electrolyte/electrode interface. The diagonal line in the low-frequency region corresponds to the diffusion process of Li^+ . The semicircular diameter of SPCNFs-5:5 in the high-frequency region is smaller than that of CNFs, due to the formation of holes that increase the specific surface area, and provide more active sites for lithium ions. At the same time, the presence of the nucleation layer increases the strength of the fiber to maximize resistance to damage caused by electrochemical reactions, providing a complete structure for the embedding and detachment and transfer of lithium ions, which is why the semicircular diameter of SPCNFs-5:5 in the high-frequency region is smaller than that of PCNFs-5:5.

There is no significant difference in the slope of the low-frequency region, indicating a similar diffusion process of Li^+ in the three types of electrode materials [40–42].

Figure 4b shows the first three turns of cyclic voltammograms obtained for the SPCNFs-5:5 at a scan rate of 0.1 mV s^{-1} over a voltage range of 0.01–3 V. There are significant differences between the first turn voltammogram and the rest of the voltammogram. In the first cycle of the reduction course of the SPCNFs-5:5 free-standing anode, a distinct cathodic peak appears near 0.75 V, indicating an irreversible reaction, i.e. the creation of an irreversible solid electrolyte interphase (SEI) layer and other side reactions [43, 44]. A plateau peak of around 0.5 V appears during the oxidation process, corresponding to the insertion of the Li^+ out of the graphite layer. The curves of the second and third circles overlap well, indicating the good structural stability and repeatability of the free-standing anode membrane [44, 45].

Figure 4c shows the charge and discharge curves for the first three, fiftieth and hundredth turns of the SPCNFs-5:5 free-standing anode at a current density of 100 mA g^{-1} . There is a discharge plateau of around 0.75 V in the first turn, corresponding to the cathodic peak in Fig. 4b. The absence of a significant discharge plateau during subsequent cycling is consistent with the work of peer researchers, and is in line with the characteristics of carbon-based anodes [4, 38, 46]. The curves of the 50th and 100th turn still overlap well, also indicating the good structural stability of the composite film [43].

Figure 5a shows the cycling performance of SPCNFs-5:5, PCNFs-5:5, and CNFs measured at a current density of 100 mA g^{-1} . The first cycle

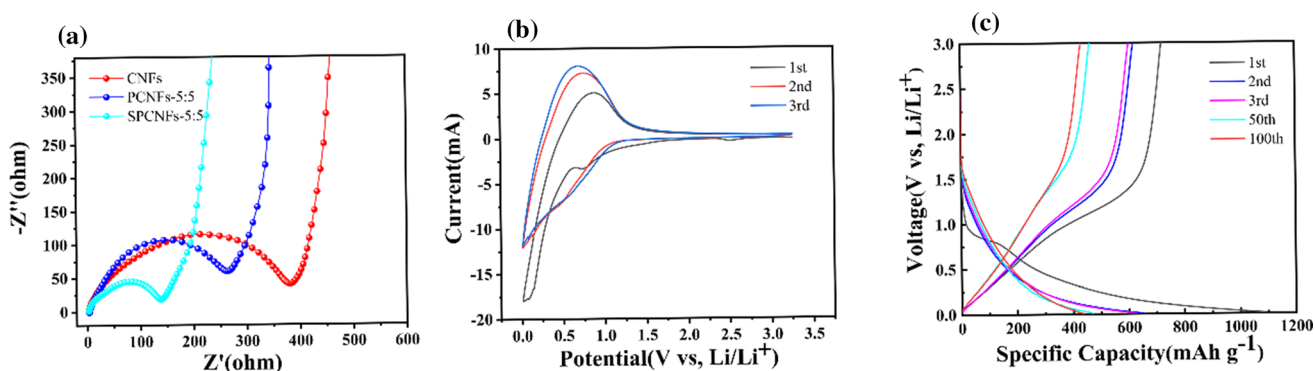


Figure 4 **a** The EIS analysis of different electrodes. **b** CV curves of SPCNFs-5:5 at 0.1 mV s^{-1} . **c** Galvanostatic charge–discharge curves of SPCNFs-5:5.

discharge capacities of SPCNFs-5:5, PCNFs-5:5, and CNFs were 1083.33, 936.43, and 342.5 mAh g⁻¹ respectively. The first cycle discharge capacity of SPCNFs-5:5, is significantly higher than that of CNFs, which is due to the porous structure of the surface providing more active sites, and allowing the electrode sheet to be in full contact with the electrolyte, which is conducive to the de-embedding of Li⁺ [22]. However, comparing with PCNFs-5:5, there is just an inconspicuous increase of initial capacity for SPCNFs-5:5. Although pores in the outer layer of SPCNFs-5:5 show an obvious trend to migrate to the surface of the fibers (which is shown in Fig. 2d, e), which could bring a little increase in specific surface area and capability to catch Li⁺, the whole outer layer porous structure of PCNFs-5:5 and SPCNFs-5:5, are inevitably similar with each other. This accounts for the phenomenon that SPCNFs-5:5 do not show a great advantage in initial capacity than PCNFs-5:5. After the first charge/discharge cycle, the amounts of SPCNFs-5:5, PCNFs-5:5, and CNFs, were 610, 518.14, and 287.92 mAh g⁻¹, respectively, with capacity retention rates of 56.31%, 55.33%, and 84.06%, respectively. It is interesting to find that the initial

discharge capacity of CNFs is small, but the capacity retention is better and significantly higher than the other two electrode materials, due to their homogeneous fiber morphology, non-porous structure, and less consumption of electrolytes. At a current density of 100 mA g⁻¹, the three-electrode materials showed good cycling stability after 100 charges/discharge cycles. The Coulomb efficiency is approximately equal to 100%, when all three electrode materials reach a steady state, indicating that the Li⁺ intercalation process is highly reversible. After 100 cycles, the discharge capacities of SPCNFs-5:5, PCNFs-5:5, and CNFs were 445.33, 354.43, and 274.17 mAh g⁻¹, respectively. The higher discharge capacity of SPCNFs-5:5 and PCNFs-5:5, compared to CNFs, is due to the ability of the pore structure to accommodate the volume changes during the reaction, and provide more active sites. Furthermore, owing to the improved mechanical properties, the surface porous while the inner dense structure of SPCNFs-5:5 can maintain better structural stability and electrochemical performance than that of PCNFs-5:5 [40, 47].

Figure 5b shows the rate performance of SPCNFs-5:5, PCNFs-5:5, and CNFs. Rate performance refers to

Figure 5 **a** Cycling performance of CNFs, PCNFs-5:5, and SPCNFs-5:5 at 100 mA g⁻¹. **b** Rate performance of CNFs, PCNFs-5:5, and SPCNFs-5:5. **c** Long-term cycling performance of CNFs, PCNFs-5:5, and SPCNFs-5:5 at 1 A g⁻¹.

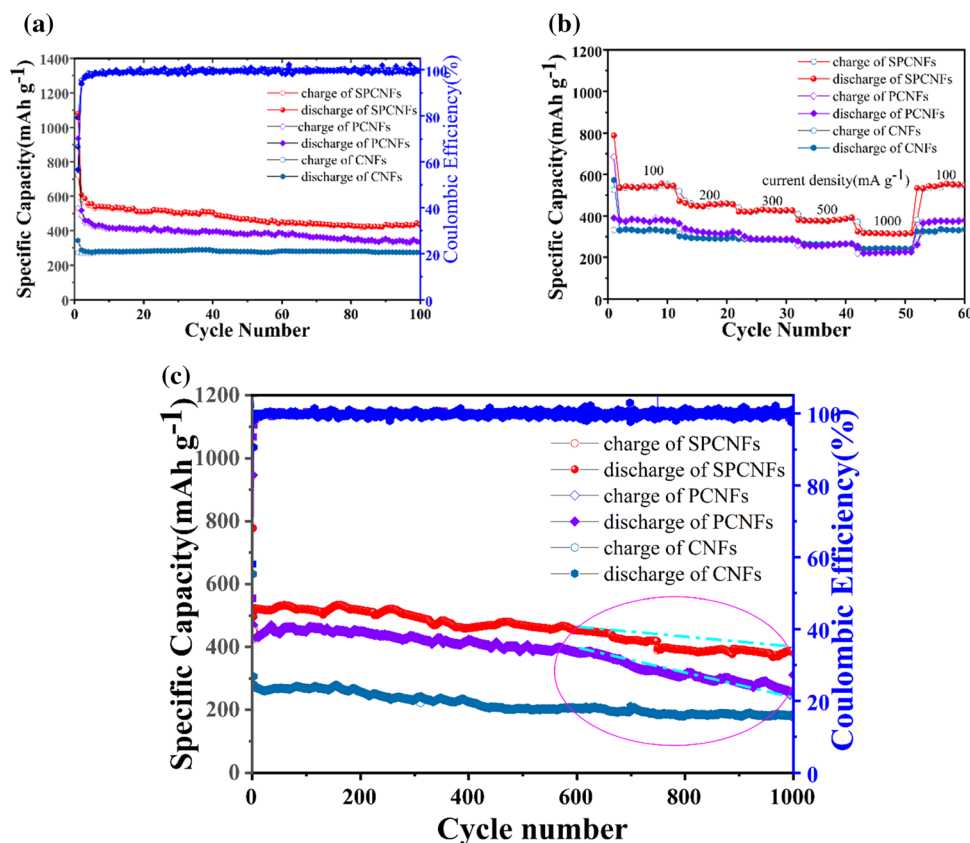
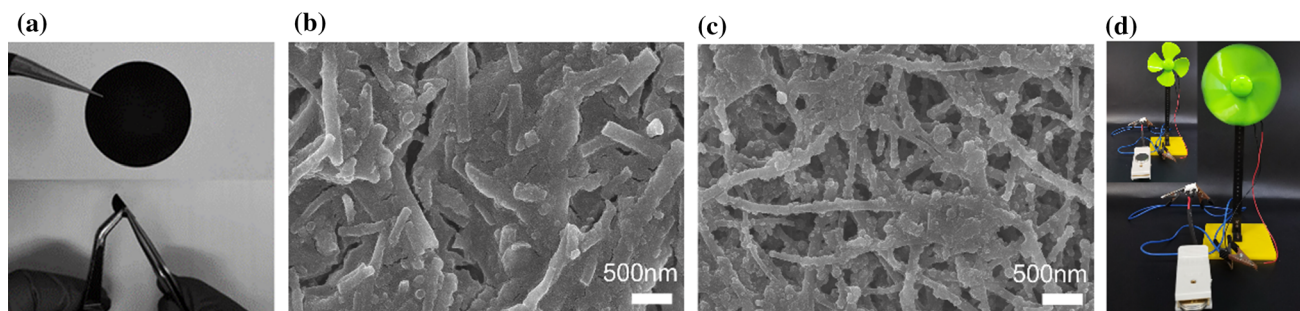


Table 1 Comparison of the capacity loss rates of the three electrode samples

Materials	Current density (mA g ⁻¹)	Initial capacity (mAh g ⁻¹)	Cycle number	Retained capacity (mAh g ⁻¹)	Capacity loss rate (%)
CNFs	1000	631.88	1000	179.38	71.62
PCNFs-5:5	1000	946.67	1000	310.66	67.18
SPCNFs-5:5	1000	777.94	1000	388.92	50.01

**Figure 6** a Digital photo and bending test inset. SEM images of the freestanding electrode after 1000 cycles at 1 A g⁻¹ b PCNFs-5:5, c SPCNFs-5:5, d Power the small fan.**Table 2** Comparison of the Capacity of SPCFs with some other porous carbon-based material

Materials	Cycle	Current density (mA g ⁻¹)	Capacity (mAh g ⁻¹)	Refs
SPCNFs-5:5	100	100	445.33	This work
	1000	1000	388.92	
Graphite			372.07	Theoretical
Bio-derived Carbon	200	124	160	[48]
PCNFs	100	200	354	[22]
N- PCNFs	500	1000	780	[46]
Hollow-PCNFs	50	50	293.7	[49]
PCNFs-@MoS ₂	50	50	736	[50]
Si@SiOx@CNFs	100	500	1104	[51]
ES-CNCo ₃ O ₄	500	2000	705	[52]
Zn-MOFsderived PCNFs	200	100	520	[53]
CoMoO ₄ /CNFs	200	200	802	[54]
TiO ₂ Sn@CNTs	1100	200	643	[55]

the magnitude, retention, and recovery of capacity exhibited at current densities. The current densities are cycled at 100, 200, 300, 500, and 1000 mA g⁻¹, in sequence, with each cycle performed 10 times. The final discharge capacities of SPCNFs-5:5 are 543.75, 460, 427.5, 392.5, 317.5 mAh g⁻¹ when the current densities are 100, 200, 300, 500, 1000 mA g⁻¹. When the current density returns to 100 mA g⁻¹, the capacity returns to 547.92 mAh g⁻¹. The excellent rate performance of SPCNFs-5:5 is due to its unique surface porous structure, which accommodates

volume changes during the reaction process, ensures efficient penetration of the electrolyte into the electrode sheet during cycling, and also tolerates multiple dislodgement and insertion of lithium ions, without damaging the electrode sheet.

The charge/discharge distribution of SPCNFs-5:5 at a high current density of 1 A g⁻¹ is shown in Fig. 5c. The initial discharge capacity of SPCNFs-5:5 is 777.94 mAh g⁻¹. After 1000 cycles, the capacity becomes 388.92 mAh g⁻¹, with a capacity retention rate of 49.99%. At a steady-state, the Coulomb

efficiency is approximately equal to 100%. The above shows that SPCNFs-5:5 has good long-cycle performance at high current densities [12]. The specific capacity decay rate of SPCNFs-5:5 1000th lap with respect to 600th lap is 14%, while the decay rate of PCNFs-5:5 1000th lap with respect to 600th lap increases to 19%. Especially after 600 cycles of charge and discharge, the LIBs with PCNFs-5:5 anode exhibit a higher fading rate than that of LIBs with SPCNFs-5:5.

We compared the capacity loss rates of the three electrode samples, as showed in Table 1. At a current density of 1000 mA g^{-1} for 1000 cycles, the capacity loss rate of SPCNFs-5:5, was 50.01% significantly smaller than that of PCNFs-5:5 and CNFs (67.18%, 71.62%), which shows significant cycling stability performance, mainly due to the surface porous structure with both abundant active sites and mechanical strength.

Figure 6a shows SPCNFs-5:5 original freestanding electrode discs with good bendability and flexibility. Figure 6b shows the SEM image of PCNFs-5:5 as an electron electrode after 1000 cycles at 1 Ag^{-1} current density, and the fibers showed a significant fracture. However, the SEM images of SPCNFs-5:5 are shown in Fig. 6c, the composite membrane structure remains relatively intact, with no significant structural changes. The excellent structural stability of SPCNFs-5:5 films ensures that they can be cycled effectively over long periods at high current densities. The SPCNFs are used as anodes to obtain a 2025 coin cell that can keep the small fan turning, which demonstrated the stable cycling capability of the battery. This once again proves that SPCNFs have practical applications.

We compared the work we did with other literature on porous carbon nanofibers, as shown in Table 2. The rate performance and long-cycle stabilities of SPCNFs-5:5 are superior to those of CNFs and PCNFs, mainly because SPCNFs-5:5 produces a porous structure, while partially retaining the mechanical strength of the fibers, which is conducive to improving structural stability. However, the performance is inferior to anode materials with metal oxides or metal particles added, which is mainly superior to metal particles or metal oxides that can act as active substances, and play a role in improving charge transfer.

Conclusions

We have successfully developed CNFs films with a surface porous structure that can be used as a free-standing anode for LIBs. Coaxial electrostatic spinning technology and template method allow simplified and controlled preparation of SPCNFs. Thanks to its unique surface porous structure, it can accommodate both the volume changes during the reaction, providing more active sites, while maximizing the retention of fiber strength and improving cycle stability. All of these contribute to a high specific capacity (610 mAh g^{-1} after 100 cycles at 100 mAh g^{-1}). Excellent rate performance can be observed (317.5 mAh g^{-1} at 1000 mA g^{-1} , $547.92 \text{ mAh g}^{-1}$ after 10 cycles at 100 mA g^{-1}). Stability at high current densities can also be guaranteed ($388.92 \text{ mAh g}^{-1}$ after 1000 cycles at 1 A g^{-1}). In conclusion, this work provides a new idea for the preparation of free-standing anodes of LIBs, which holds great promise for simplifying the process, increasing capacity, and improving cycle stability.

Acknowledgements

This work was supported by China Postdoctoral Science Foundation (2018M640240 and 2019T120189).

Declarations

Conflict of interest No conflict of interest in the submission of this manuscript and the manuscript is approved by all authors for publication.

References

- [1] Sun YM, Liu NA, Cui Y (2016) Promises and challenges of nanomaterials for lithium-based rechargeable batteries. *Nat Energy*. <https://doi.org/10.1038/Nenergy.2016.71>
- [2] Wan J, Xie J, Kong X et al (2019) Ultrathin, flexible, solid polymer composite electrolyte enabled with aligned nanoporous host for lithium batteries. *Nat Nanotechnol* 14:705–711. <https://doi.org/10.1038/s41565-019-0465-3>
- [3] Chen RZ, Hu Y, Shen Z et al (2017) Facile fabrication of foldable electrospun polyacrylonitrile-based carbon nanofibers for flexible lithium-ion batteries. *J Mater Chem A* 5:12914–12921. <https://doi.org/10.1039/c7ta02528a>
- [4] Huang L, Guan Q, Cheng JL et al (2018) Free-standing N-doped carbon nanofibers/carbon nanotubes hybrid film for

- flexible, robust half and full lithium-ion batteries. *Chem Eng J* 334:682–690. <https://doi.org/10.1016/j.cej.2017.10.030>
- [5] Cheong JY, Benker L, Zhu J et al (2019) Generalized and feasible strategy to prepare ultra-porous, low density, compressible carbon nanoparticle sponges. *Carbon* 154:363–369. <https://doi.org/10.1016/j.carbon.2019.08.021>
- [6] Chiang YC, Wu CY, Chen YJ (2020) Effects of activation on the properties of electrospun carbon nanofibers and their adsorption performance for carbon dioxide. *Sep Purif Technol.* <https://doi.org/10.1016/j.seppur.2019.116040>
- [7] Wang Y, Raman Pillai SK, Che J, Chan-Park MB (2017) High interlaminar shear strength enhancement of carbon fiber/epoxy composite through fiber- and matrix-anchored carbon nanotube networks. *ACS Appl Mater Interfaces* 9:8960–8966. <https://doi.org/10.1021/acsami.6b13197>
- [8] Yang FH, Hu GM, He HY et al (2019) Effect of amorphous carbon on the tensile behavior of polyacrylonitrile (PAN)-based carbon fibers. *J Mater Sci* 54:8800–8813. <https://doi.org/10.1007/s10853-018-03256-z>
- [9] Lv P, Feng YY, Zhang P, Chen HM, Zhao NQ, Feng W (2011) Increasing the interfacial strength in carbon fiber/epoxy composites by controlling the orientation and length of carbon nanotubes grown on the fibers. *Carbon* 49:4665–4673. <https://doi.org/10.1016/j.carbon.2011.06.064>
- [10] Im JS, Park SJ, Kim TJ, Kim YH, Lee YS (2008) The study of controlling pore size on electrospun carbon nanofibers for hydrogen adsorption. *J Colloid Interface Sci* 318:42–49. <https://doi.org/10.1016/j.jcis.2007.10.024>
- [11] Chen TQ, Liu Y, Pan LK et al (2014) Electrospun carbon nanofibers as anode materials for sodium ion batteries with excellent cycle performance. *J Mater Chem A* 2:4117–4121. <https://doi.org/10.1039/c3ta14806h>
- [12] Wang A, Xie SM, Zhang R et al (2019) Chemical vapor deposition growth of carbon nanotube confined nickel sulfides from porous electrospun carbon nanofibers and their superior lithium storage properties. *Nano Adv* 1:656–663. <https://doi.org/10.1039/c8na00234g>
- [13] Weng W, Kurihara R, Wang J, Shiratori S (2019) Electrospun carbon nanofiber-based composites for lithium-ion batteries: structure optimization towards high performance. *Compos Commun* 15:135–148. <https://doi.org/10.1016/j.coco.2019.07.005>
- [14] Jiang WW, Liu QH, Peng JF, Jiang YH, Ding YH, Wei Q (2020) Co₉S₈ nanoparticles embedded into amorphous carbon as anode materials for lithium-ion batteries. *Nanotechnology* 31:8. <https://doi.org/10.1088/1361-6528/ab7887>
- [15] Yu MK, Sun YX, Du HR et al (2019) Hollow porous carbon spheres doped with a low content of Co₃O₄ as anode materials for high performance lithium-ion batteries. *Electrochim Acta* 317:562–569. <https://doi.org/10.1016/j.electacta.2019.06.027>
- [16] Wu DB, Ouyang YR, Zhang WL et al (2020) Hollow cobalt oxide nanoparticles embedded porous reduced graphene oxide anode for high performance lithium ion batteries. *Appl Surf Sci* 508:8. <https://doi.org/10.1016/j.apsusc.2020.145311>
- [17] Zhai XM, Xu XM, Zhu XL, Zhao YJ, Li JB, Jin HB (2018) Porous layer assembled hierarchical Co₃O₄ as anode materials for lithium-ion batteries. *J Mater Sci* 53:1356–1364. <https://doi.org/10.1007/s10853-017-1579-3>
- [18] Wang J, Zhou YK, Hu YY, O’Hayre R, Shao ZP (2013) Porous nanocrystalline TiO₂ with high lithium-ion insertion performance. *J Mater Sci* 48:2733–2742. <https://doi.org/10.1007/s10853-012-7073-z>
- [19] Zhao PF, Li W, Fang SQ, Yu J, Yang ZY, Cai JX (2019) Cut-price fabrication of free-standing porous carbon nanofibers film electrode for lithium-ion batteries. *Appl Sci-Basel.* <https://doi.org/10.3390/app9051016>
- [20] Cavaliere S, Subianto S, Savych I, Jones DJ, Roziere J (2011) Electrospinning: designed architectures for energy conversion and storage devices. *Energy Environ Sci* 4:4761–4785. <https://doi.org/10.1039/c1ee02201f>
- [21] Oh JH, Jo MS, Jeong SM, Cho C, Kang YC, Cho JS (2019) New synthesis strategy for hollow NiO nanofibers with interstitial nanovoids prepared via electrospinning using camphene for anodes of lithium-ion batteries. *J Ind Eng Chem* 77:76–82. <https://doi.org/10.1016/j.jiec.2019.04.021>
- [22] Peng YT, Lo CT (2015) Electrospun porous carbon nanofibers as lithium ion battery anodes. *J Solid State Electrochem* 19:3401–3410. <https://doi.org/10.1007/s10008-015-2976-7>
- [23] Zheng GF, Peng H, Jiang JX et al (2021) Surface functionalization of PEO Nanofibers using a TiO₂ suspension as sheath fluid in a modified coaxial electrospinning process. *Chem Res Chinese Univ* 37:571–577. <https://doi.org/10.1007/s40242-021-1118-2>
- [24] Feng XS, Luo FQ, Chen YY et al (2021) Boosting total oxidation of propane over CeO₂@Co₃O₄ nanofiber catalysts prepared by multifluidic coaxial electrospinning with continuous grain boundary and fast lattice oxygen mobility. *J Hazard Mater* 406:12. <https://doi.org/10.1016/j.jhazmat.2020.124695>
- [25] Liu X, Jiang YH, Li KF, Xu F, Zhang P, Ding YH (2019) Electrospun free-standing N-doped C@SnO₂ anode paper for flexible Li-ion batteries. *Mater Res Bull* 109:41–48. <https://doi.org/10.1016/j.materresbull.2018.09.023>
- [26] Yu H, Chen L, Li WX, Dirican MM, Liu Y, Zhang XW (2021) Root-whisker structured 3D CNTs-CNFs network based on coaxial electrospinning: a free-standing anode in lithium-ion batteries. *J Alloy Compd* 863:9. <https://doi.org/10.1016/j.jallcom.2020.158481>

- [27] Chen NN, Chen L, Li WX, Xu ZW, Qian XM, Liu Y (2019) Brush-like Ni/carbon nanofibers/carbon nanotubes multi-layer network for freestanding anode in lithium ion batteries. *Ceram Int* 45:16676–16681. <https://doi.org/10.1016/j.ceramint.2019.05.108>
- [28] Li C, Li Q, Ni X, Liu G, Cheng W, Han G (2017) Coaxial electrospinning and characterization of core-shell structured cellulose nanocrystal reinforced PMMA/PAN Composite fibers. *Materials* 10:572. <https://doi.org/10.3390/ma10060572>
- [29] Huang J, Cao Y, Huang Z et al (2016) Comparatively thermal and crystalline study of poly(methyl-methacrylate)/polyacrylonitrile hybrids: core-shell hollow fibers, porous fibers, and thin films. *Macromol Mater Eng* 301:1327–1336. <https://doi.org/10.1002/mame.201600172>
- [30] Yan K, Kong L-B, Dai Y-H et al (2015) Design and preparation of highly structure-controllable mesoporous carbons at the molecular level and their application as electrode materials for supercapacitors. *J Mater Chem A* 3:22781–22793. <https://doi.org/10.1039/c5ta05947j>
- [31] Lee BS (2020) A review of recent advancements in electrospun anode materials to improve rechargeable lithium battery performance. *Polymers (Basel)*. <https://doi.org/10.3390/polym12092035>
- [32] Shilpa DSK, Afzal MAF, Srivastava S, Patil S, Sharma A (2016) Enhanced electrical conductivity of suspended carbon nanofibers: effect of hollow structure and improved graphitization. *Carbon* 108:135–145. <https://doi.org/10.1016/j.carbon.2016.06.103>
- [33] Ran F, Shen K, Tan Y et al (2016) Activated hierarchical porous carbon as electrode membrane accommodated with triblock copolymer for supercapacitors. *J Membr Sci* 514:366–375. <https://doi.org/10.1016/j.memsci.2016.05.011>
- [34] Borhani S, Zadhoush A, Fathi M (2020) Mechanical properties of transparent poly(methyl methacrylate) nanocomposites reinforced with core-shell polyacrylonitrile/poly(methyl methacrylate) nanofibers. *J Appl Polym Sci*. <https://doi.org/10.1002/app.49192>
- [35] Choi H, No P, Lee Y-J, Choi J-H (2017) A pore-structured Si alloy anode using an unzipping polymer for a lithium ion battery. *J Appl Electrochem* 47:1127–1136. <https://doi.org/10.1007/s10800-017-1107-9>
- [36] Cao J, Zhao W, Gao S (2018) Properties and structure of in situ transformed PAN-based carbon fibers. *Materials (Basel)*. <https://doi.org/10.3390/ma11061017>
- [37] Du B, Chen C, Sun Y et al (2020) Lignin bio-oil-based electrospun nanofibers with high substitution ratio property for potential carbon nanofibers applications. *Polym Testing*. <https://doi.org/10.1016/j.polymertesting.2020.106591>
- [38] Huang J, Lin Y, Ji M et al (2020) Nitrogen-doped porous carbon derived from foam polystyrene as an anode material for lithium-ion batteries. *Appl Surf Sci*. <https://doi.org/10.1016/j.apsusc.2019.144398>
- [39] Shilpa S, Sharma A (2016) Free standing hollow carbon nanofiber mats for supercapacitor electrodes. *RSC Adv* 6:78528–78537. <https://doi.org/10.1039/c6ra17014e>
- [40] Zhao P, Li W, Fang S, Yu J, Yang Z, Cai J (2019) Cut-price fabrication of free-standing porous carbon nanofibers film electrode for lithium-ion batteries. *Appl Sci*. <https://doi.org/10.3390/app9051016>
- [41] Zeng Y, Huang Y, Liu N et al (2021) N-doped porous carbon nanofibers sheathed pumpkin-like Si/C composites as free-standing anodes for lithium-ion batteries. *J Energy Chem* 54:727–735. <https://doi.org/10.1016/j.jechem.2020.06.022>
- [42] Du Z, Ai W, Yu C et al (2019) A facile grinding approach to embed red phosphorus in N, P-codoped hierarchical porous carbon for superior lithium storage. *Sci China Mater* 63:55–61. <https://doi.org/10.1007/s40843-019-9499-2>
- [43] Xu Z, Fan L, Ni X, Han J, Guo R (2019) Sn-encapsulated N-doped porous carbon fibers for enhancing lithium-ion battery performance. *RSC Adv* 9:8753–8758. <https://doi.org/10.1039/c8ra10201e>
- [44] Liang G, Qin X, Zou J et al (2018) Electrospayed silicon-embedded porous carbon microspheres as lithium-ion battery anodes with exceptional rate capacities. *Carbon* 127:424–431. <https://doi.org/10.1016/j.carbon.2017.11.013>
- [45] Kong X, Zheng Y, Wang Y, Liang S, Cao G, Pan A (2019) Necklace-like Si@C nanofibers as robust anode materials for high performance lithium ion batteries. *Science Bulletin* 64:261–269. <https://doi.org/10.1016/j.scib.2019.01.015>
- [46] Xie WH, Gu LL, Li SY et al (2017) Polydopamine derived porous N-doped carbon nanofibers for lithium ion storage. *Mater Lett* 189:259–262. <https://doi.org/10.1016/j.matlet.2016.12.017>
- [47] Niu H, Zhang J, Xie Z, Wang X, Lin T (2011) Preparation, structure and supercapacitance of bonded carbon nanofiber electrode materials. *Carbon* 49:2380–2388. <https://doi.org/10.1016/j.carbon.2011.02.005>
- [48] Hernandez-Rentero C, Marangon V, Olivares-Marin M et al (2020) Alternative lithium-ion battery using biomass-derived carbons as environmentally sustainable anode. *J Colloid Interface Sci* 573:396–408. <https://doi.org/10.1016/j.jcis.2020.03.092>
- [49] Lei WW, Liu S, Zhang WH (2017) Porous hollow carbon nanofibers derived from multi-walled carbon nanotubes and sucrose as anode materials for lithium-ion batteries. *RSC Adv* 7:224–230. <https://doi.org/10.1039/c6ra24927b>
- [50] Miao YE, Huang YP, Zhang LS, Fan W, Lai FL, Liu TX (2015) Electrospun porous carbon nanofiber@MoS₂ core/

- sheath fiber membranes as highly flexible and binder-free anodes for lithium-ion batteries. *Nanoscale* 7:11093–11101. <https://doi.org/10.1039/c5nr02711j>
- [51] Zhou XS, Wan LJ, Guo YG (2013) Electrospun silicon nanoparticle/porous carbon hybrid nanofibers for lithium-ion batteries. *Small* 9:2684–2688. <https://doi.org/10.1002/sml.201202071>
- [52] Zhang CL, Lu BR, Cao FH, Yu ZL, Cong HP, Yu SH (2018) Hierarchically structured Co₃O₄@carbon porous fibers derived from electrospun ZIF-67/PAN nanofibers as anodes for lithium ion batteries. *J Mater Chem A* 6:12962–12968. <https://doi.org/10.1039/c8ta03397h>
- [53] Zheng GX, Chen MH, Zhang HR et al (2019) Zn-MOFs derived porous carbon nanofiber for high performance lithium-ion batteries. *Surf Coat Technol* 359:384–389. <https://doi.org/10.1016/j.surfcoat.2018.12.075>
- [54] Xie SM, Wang HK, Yao TH et al (2019) Embedding CoMoO₄ nanoparticles into porous electrospun carbon nanofibers towards superior lithium storage performance. *J Colloid Interface Sci* 553:320–327. <https://doi.org/10.1016/j.jcis.2019.06.039>
- [55] Mao ML, Yan FL, Cui CY et al (2017) Pipe-wire TiO₂-Sn@carbon nanofibers paper anodes for lithium and sodium ion batteries. *Nano Lett* 17:3830–3836. <https://doi.org/10.1021/acs.nanolett.7b01152>

Publisher's Note Springer Nature remains neutral with regard to jurisdictional claims in published maps and institutional affiliations.